Chiral J-Aggregates of Atropo-Enantiomeric Perylene Bisimides and Their Self-Sorting Behavior

ARTICLE *in* CHEMISTRY - A EUROPEAN JOURNAL · JUNE 2012

Impact Factor: 5.73 · DOI: 10.1002/chem.201200089 · Source: PubMed

4 AUTHORS, INCLUDING:

Vladimir Stepanenko
University of Wuerzburg
65 PUBLICATIONS **2,001** CITATIONS
SEE PROFILE

Krzysztof Radacki
University of Wuerzburg
271 PUBLICATIONS **5,435** CITATIONS
SEE PROFILE

CHEMISTRY
A EUROPEAN JOURNAL

ChemPubSoc
Europe

DOI: 10.1002/chem.201200089

VIP

Chiral J-Aggregates of Atropo-Enantiomeric Perylene Bisimides and Their Self-Sorting Behavior

Zengqi Xie,[a] Vladimir Stepanenko,[a] Krzysztof Radacki,[b] and Frank Würthner*[a]

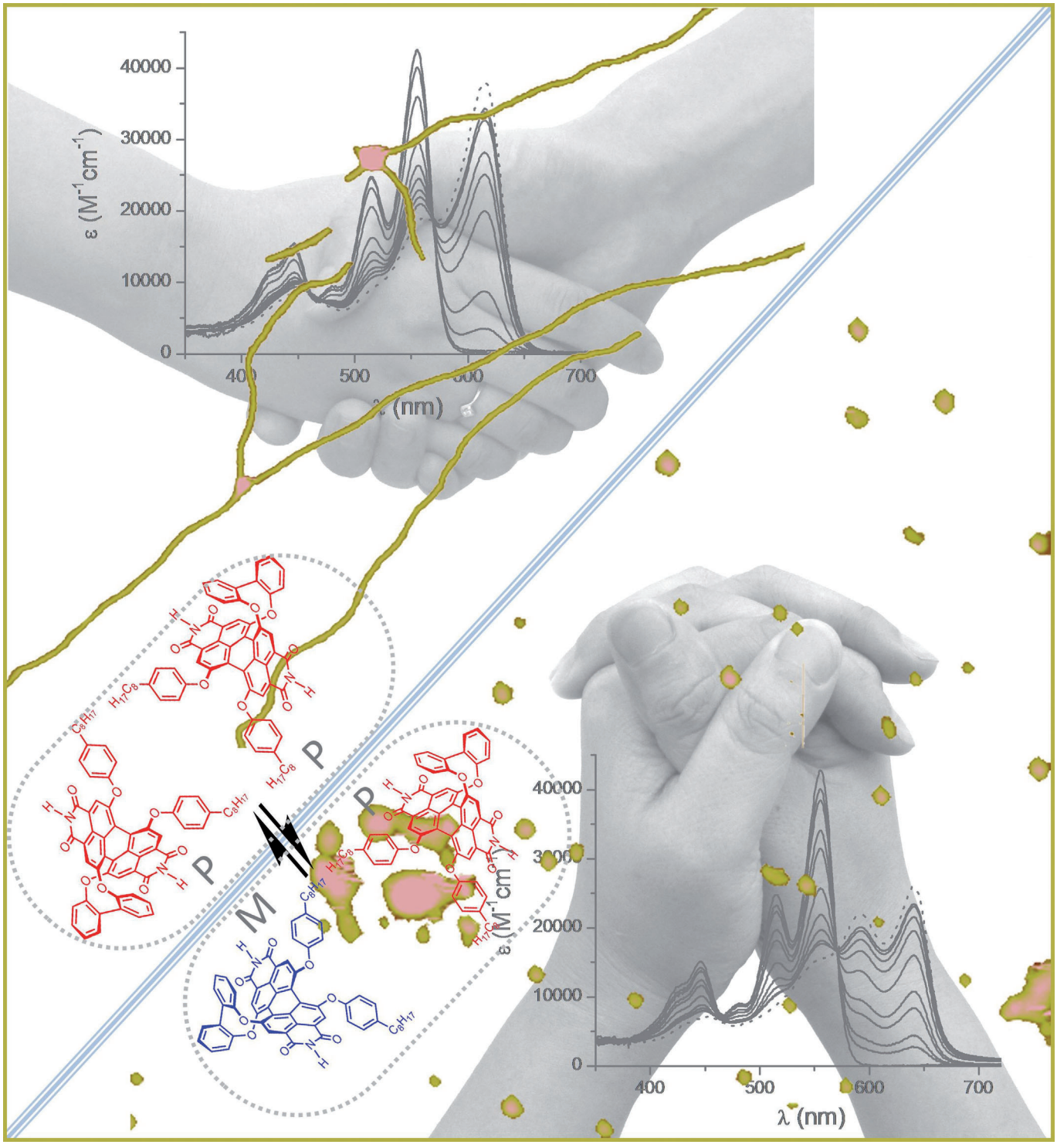

Abstract: Herein we report on structural, morphological, and optical properties of homochiral and heterochiral J-aggregates that were created by nucleation–elongation assembly of atropo-enantiomerically pure and racemic perylene bisimides (PBIs), respectively. Our detailed studies with conformationally stable biphenoxy-bridged chiral PBIs by UV/Vis absorption, circular dichroism (CD) spectroscopy, and atomic force microscopy (AFM) revealed structurally as well as spectroscopically quite different kinds of J-aggregates for enantiomerically pure and racemic PBIs. AFM investigations showed that enantiopure PBIs form helical nanowires of unique diameter and large length-to-width ratio by self-recognition, while racemic PBIs provide irregular-sized particles by self-discrimination of the enantiomers at the stage of nucleation. Steady-state fluorescence spectroscopy studies revealed that the photoluminescence efficiency of homochiral J-aggregated nanowires ($47\pm3\%$) is significantly higher than that of heterochiral J-aggregated particle-like aggregates ($12\pm3\%$), which is explained in terms of highly ordered molecular stacking in one-dimensional nanowires of homochiral J-aggregates. Our present results demonstrate the high impact of homochirality on the construction of well-defined nanostructures with unique optical properties.

Keywords: chirality · helical nanowires · J-aggregates · perylene bisimide · self-assembly

Introduction

J-aggregates have been a subject of intensive research work during the last decades owing to their unique optical properties such as red-shifted absorption bands with respect to those of the respective monomers, superradiance, and their ability to delocalize and migrate excitons.[1] Some recent highlights in this field are fluorescence-based biosensing by peptide-templated cyanine J-aggregate developed by Whitten and co-workers,[2] photoinduced reduction of noble metal ions into metal nanowires in templates of tubular J-aggregates reported by Eisele et al.,[3] and single molecule spectroscopy of individual J-aggregates.[4] In the context of this work, it is interesting to mention that chiral J-aggregates have also been studied, for example, from cyanines,[5] porphyrins,[6] chlorines,[7] and perylene bisimides,[8] which were either prepared from such dye systems that contain chiral peripheral substituents or induced by chiral additives. For those systems, typically a chiral bias—however, usually far less than quantitative—is achieved towards a preferred handedness of helical aggregates.[9]

In principle, J-aggregates are a special, particularly interesting case of self-assembled organic materials. Self-assembly is, on the other hand, a powerful strategy for organizing π-conjugated molecular building blocks into functional chiral as well as achiral aggregates.[10] Conjugated π-systems containing chiral substituents usually show quite different aggregation behavior when compared with their racemates.[11] Molecules of a single handedness typically generate one-dimensional helical nanofibers, which show enhanced chiroptical properties arising from the coupling between the transition dipole moments due to the helical molecular displacement.[11] It has been recognized already some years ago that the introduction of bulky substituents at the bay area of perylene bisimide (PBI) leads to a twist of the perylene core that results in inherently chiral π-surfaces by symmetry breaking.[12] However, the isolation of pure atropo-enantiomeric PBIs (*M* and *P* enantiomers) has been difficult in most cases due to low barriers of dynamic interconversions of the enantiomers.[13] In the past years, our research group has succeeded to resolve the atropo-enantiomers of PBIs either by increasing the size of the sterically more demanding bay substituents,[13] or by bridging phenoxy substituents at the bay positions with oligo(ethylene glycol) chains through macrocyclization.[14] Recent studies on self-sorting[15] of oligo(ethylene glycol) tethered chiral PBI dyes have revealed that self-recognition prevails over self-discrimination, and thus preferentially homochiral dimer are formed with H-type aggregation owing to the stronger π–π binding strength between homochiral π-surfaces.[16a] Most recently, we have accomplished the synthesis of conformationally stable, core-twisted chiral PBIs that bear a rigid 2,2′-biphenoxy bridge at one bay area.[17] The easy separation of the enantiomers of such rigid, chiral PBI derivatives at room temperature enables us to develop homochiral supramolecular building blocks of this very important class of functional π-conjugated dyes.[18]

It has been reported previously that the introduction of NH groups at the imide positions of core-twisted PBIs results in the formation of one-dimensional J-aggregates due to the slipped face-to-face arrangement by the mutual effects of hydrogen bonding, π–π interaction and core-twisted structure.[19] However, to the best of our knowledge, homochiral J-aggregates of intrinsically chiral π-conjugated aromatic systems, that is, those with chiral core, are not known to date. To achieve such homochiral J-aggregates, we have

[a] Dr. Z. Xie, Dr. V. Stepanenko, Prof. Dr. F. Würthner
Universität Würzburg
Institut für Organische Chemie and
Center for Nanosystems Chemistry
Am Hubland, 97074 Würzburg (Germany)
Fax: (+49) 931-31-84756
E-mail: wuerthner@chemie.uni-wuerzburg.de

[b] Dr. K. Radacki
Universität Würzburg
Institut für Anorganische Chemie
Am Hubland, 97074 Würzburg (Germany)

Supporting information for this article is available on the WWW under http://dx.doi.org/10.1002/chem.201200089.

designed and synthesized the unique kind of chiral PBI **4** that contains a 2,2′-biphenoxy bridge at one bay area and hydrogen atoms in the imide positions to direct intermolecular hydrogen bonding (for the structure, see Scheme 1). We have studied the self-sorting behavior of the atropo-enantiomerically pure and racemic PBIs **4**, revealing that self-discrimination prevails over self-recognition for the racemate, leading to ill-defined nanostructures. In contrast, self-recognition of the enantiopure PBIs **4** (*M*-**4** or *P*-**4**) afforded well-defined helical nanowires that constitute the first examples of homochiral PBI J-aggregates.

Results and Discussion

Synthesis and chiral resolution of the atropo-enantiomers of PBI: Our newly designed target compound chiral PBI **4** that contains hydrogen atoms at the imide positions was synthesized according to the route outlined in Scheme 1. Tetrachloro-substituted PBI **1** bearing α-methylbenzyl groups at the imide positions was used as a starting material, which was synthesized according to our previously reported method.[19] The nucleophilic substitution of two chlorine atoms at one bay area of PBI **1** with 2,2′-biphenol (with a mole ratio of 1:1.1) afforded PBI **2** with one biphenoxy bridge in the bay area. The further nucleophilic substitution of the two chlorine atoms of PBI **2** with 4-octylphenol (mole ratio of 1:3) provided PBI **3** in 42% yield. Subsequent saponification of PBI **3** with potassium hydroxide in *t*BuOH at 80°C, followed by treatment with glacial acetic acid at room temperature gave the corresponding perylene bisanhydride, which was used without further purification for the imidization with excess amount of ammonium acetate in propionic acid at 140°C to afford our target PBI **4** in a total yield of 82% for the two steps. PBI **4** with two unsymmetrically substituted bay areas and rigid core scaffold imparted by the biphenoxy bridge is well soluble in common organic solvents such as THF, chloroform, dichloromethane, and toluene, but it is modestly soluble in aliphatic solvents like methylcyclohexane (MCH). For the detailed characterization data of the hitherto unknown PBI **4**, see the Experimental Section.

The sterically demanding substituents of the bay area of PBI **4** should lead to a twist of the aromatic core, and thus a racemate (*rac*-**4**) composing of atropisomeric *P*-enantiomer (*P*-**4**) and *M*-enantiomer (*M*-**4**) was obtained. The 2,2′-biphenoxy bridge in one bay area of PBI **4** makes the chiral π-core rigid and thus imparts conformational stability, facilitating the resolution of the atropo-enantiomers of this PBI at room temperature.[17] Due to the high free activation enthalpy value of biphenoxy-bridged PBI **4** ($\Delta G^{\neq}_{333K} = 99.8\ kJ\,mol^{-1}$), the racemization of isolated enantiopure PBI **4** in solution is much slower compared to that of conformationally flexible, at bay area tetraphenoxy-substituted PBI (ca. 60 $kJ\,mol^{-1}$),[13] and the racemization process of PBI **4** is totally prohibited in aggregates by intermolecular interactions between core-twisted PBI molecules (see the Supporting Information for details). As shown in Figure 1, the enantiomers of *rac*-**4** could be perfectly separated by HPLC using a chiral column and chloroform as eluent. The absolute configurations of the first and second eluted atropo-

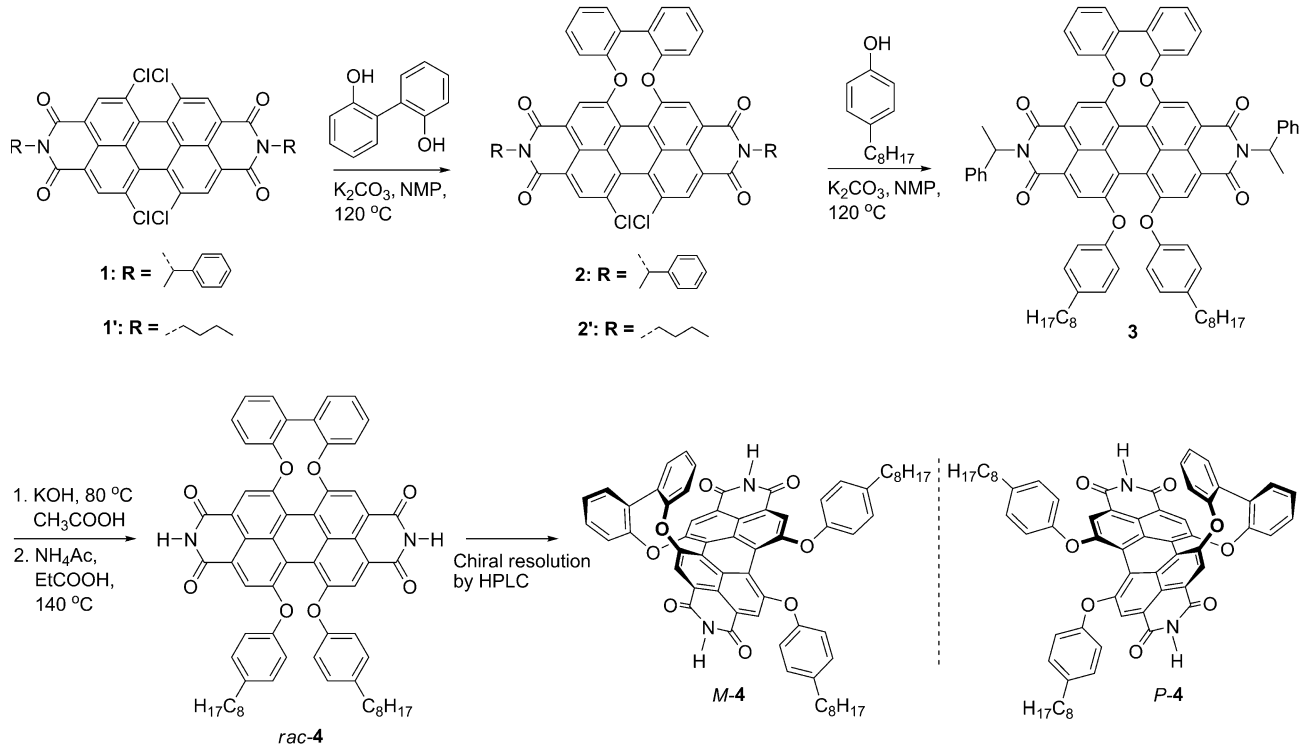

Scheme 1. Synthesis and chiral resolution of PBI **4**. NMP = *N*-methyl-2-pyrrolidone.

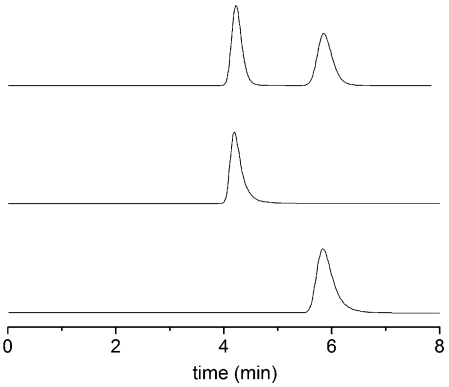

Figure 1. HPLC chromatograms before (top) and after (middle and bottom) separation of the atropo-enantiomers of *rac*-**4** on a Trentec Reprosil 100 chiral-NR column (Ø = 0.8 cm) at ambient conditions using chloroform as eluent (flow rate: 1 mL min^{-1}).

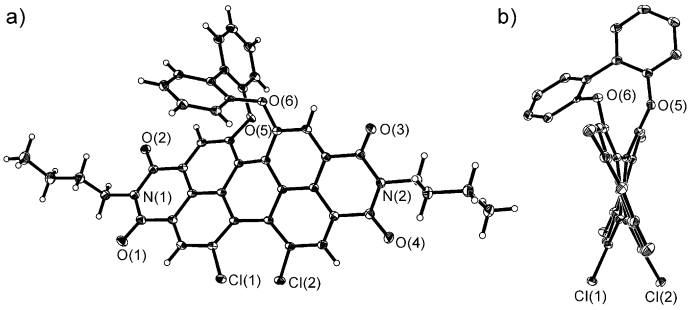

Figure 2. Molecular structure of PBI **2′** (*P*-enantiomer is shown) determined by single crystal X-ray analysis; a) top view and b) view along N–N axis. The ellipsoid possibility is 35 %. The alkyl chains and hydrogen atoms are omitted in (b) for clarity.

enantiomers (retention times 4.2 min and 5.8 min) were assigned to *P* and *M*, respectively, by comparing their CD spectra (see below) with those of the previously reported enantiomerically pure core-twisted PBIs.[14]

Molecular structural features: To get deeper insight into the molecular structure of PBI **4**, the single crystal of racemic PBI **2′** was prepared (the latter contains a 2,2′-biphenoxy bridge in the bay area as in PBI **4**). As shown in Figure 2, PBI **2′** possesses a totally unsymmetric molecular structure, not only come from the different substituents in two bay areas (one bay area is substituted by biphenoxy bridge, while the other one is occupied by two chlorine atoms) but also from the spatial orientation of the biphenoxy bridge. The feature of the spatial orientation of the biphenoxy bridge is that one phenyl ring (linked to O(6) shown in Figure 2) of the biphenoxy bridge is situated closely above the perylene π-surface, while the other one (linked to O(5)) extends to the side of the perylene core. As expected, the perylene core is twisted with a dihedral angle of 33° between the two naphthalene planes, which is between the corresponding torsional angles in tetrachloro-substituted PBIs (37°)[20] and tetraphenoxy-substituted diazadibenzoperylene derivative (25°).[21] Thus, the dihedral angle for PBI **4** should be between 33° and 25° owing to the less sterical congestion of two aryloxy substituents at one bay area of PBI **4** compared with the sterically more demanding chlorine atoms in PBI **2′**.

The spatial orientation of the biphenoxy bridge in PBI **4** is similar to that in PBI **2′** as revealed by ^{1}H NMR data shown in Figure 3. The signals for the protons on biphenoxy unit range from 7.7 ppm to 6.2 ppm (red), and there are large differences between the protons on the two bridged phenoxy substituents. Especially, the signal of proton b1 is shifted to up-field compared to that of proton b8, which indicates different surroundings for them, that is, different shielding effect from the aromatic perylene core. From the shielding effect of the perylene core on the protons of biphenoxy bridge, we can conclude that one of the phenyl rings of this bridge is situated above one of the π-surfaces of the perylene core, while the other one extends to the side of the perylene core, just the same as concluded from the single crystal of PBI **2′**. Obviously, the spatial orientation of the biphenoxy bridge has different effects on the four protons of the perylene core and on the two protons of imide groups as well, which results in six nicely separated signals in the range from 8.8 ppm to 7.7 ppm as shown in Figure 3. Accordingly, the spatial orientation of the biphenoxy bridge endows the perylene core with intrinsic chirality and two distinct π-surfaces, a shielded and a free one.

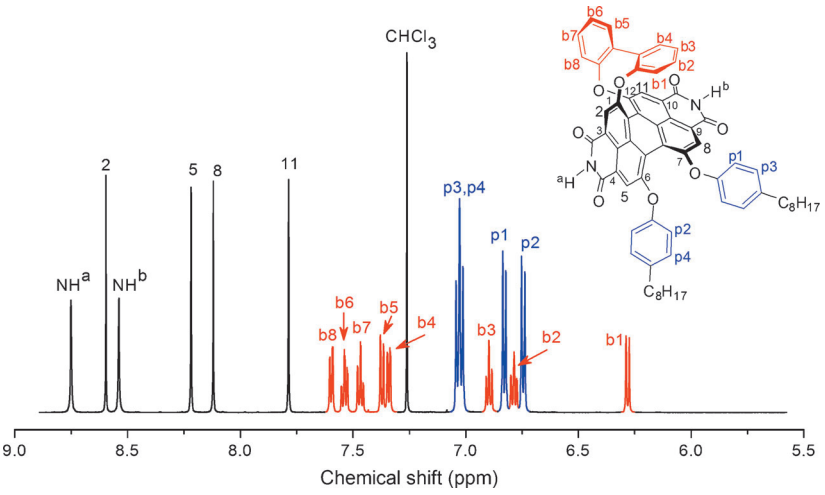

Figure 3. A section of the ^{1}H NMR spectrum (600 MHz) of *rac*-**4** in $CDCl_3$ (c = 45 mM) at ambient conditions. The assignment of ^{1}H NMR signals of PBI **4** was made according to HH-COSY NMR (see Figure S1 in the Supporting Information). Only *M*-enantiomer is shown in the inset.

Absorption properties: Figure 4a and c show the concentration-dependent absorption spectra of enantiopure *M*-**4** and *rac*-**4** in MCH, respectively. At very low concentrations ($<10^{-7}$ M), PBI **4** is molecularly dissolved in MCH. The spectra exhibit fine vibronic progressions compared with that of unbridged flexible tetraphenoxy-substituted PBIs,[22] which confirms the rigid perylene core structure of PBI **4**. With increasing concentration both *M*-**4** (or *P*-**4**) and *rac*-**4** show new red-shifted absorption bands, which clearly indicates the formation of J-aggregates. There is one intense J-band located at 615 nm for the aggregate of *M*-**4** with a shoulder at approximately 550 nm (Figure 4a), while there are two absorption bands located at 591 nm and 640 nm for the aggregate of *rac*-**4** (Figure 4c). The obvious spectral differences for the aggregates of *M*-**4** and *rac*-**4** imply distinctive packing arrangements of the dyes in the respective aggregates.

The concentration-dependent absorption spectra were utilized for an analysis of the aggregation behavior for *M*-**4** and *rac*-**4** by plotting the experimental absorption data against the total concentrations c_T as shown in Figure 4b and d, respectively; here c_T is the total concentration of initially dissolved monomeric dye molecules.[23] It is known that the aggregate formation in solution can be ascribed to chemical equilibrium between monomeric and aggregated species. If there are more than two aggregated species, multiple equilibrium may exist in the system.

$$\text{Monomer} \overset{K_2}{\rightleftharpoons} \text{Dimer} \overset{K_3}{\rightleftharpoons} \text{Trimer} \cdots\cdots \overset{K_n}{\rightleftharpoons} n\text{-mer}$$

To simplify the aggregation model and in agreement with our earlier work,[19b] we apply equilibrium constants $K_2/\sigma = K_3 = K_4 \ldots\ldots = K_n = K$.[24] The value of σ reflects the easier or more difficult formation of dimers (nucleation) and the equilibrium constants for the elongation (addition of one monomer to a dimer or to a larger aggregated species) are equal for all.[24] For cooperative, isodesmic, and anti-cooperative growth, the values of $\sigma < 1$, $\sigma = 1$, and $\sigma > 1$ are expected, respectively.[25] The fraction of aggregated molecules α_{agg} can be plotted as a function of Kc_T with any given σ values according to cooperative nucleation-elongation model ($\sigma < 1$) as the curves in Figure 4b and d show. By manual fitting of the plots of experimental absorption data to the curves for a best match, the values for σ, K, and K_2 were determined for the aggregation of *M*-**4** and *rac*-**4**, and are listed in Table 1. It can be seen that the equilibrium constants for the elongation (K) are very similar for the aggregation of *M*-**4** and *rac*-**4**, while the equilibrium constants for the nucleation (K_2) are quite different. The nucleation equilibrium constant for the racemate ($K_2 = 6.3 \times 10^4$, heterodimerization) is about twenty times larger than that of the enantiopure compounds ($K_2 = 2.7 \times 10^3$, homodimerization), which indicates stronger intermolecular interactions between the *M*-**4** and *P*-**4** molecules in heterodimer in comparison with the interactions between two *M*-**4** molecules in homodimer. This result clearly corroborates our previous model for a nucleus of two PBI molecules arranged in a slipped π-stack[19b] since for the other possibility, that is a hydrogen-bonded dimer nucleus, equal binding constants for *M*-**4**•*P*-**4** (hetero) and *M*-**4**•M-**4** (homo) nuclei are expected.

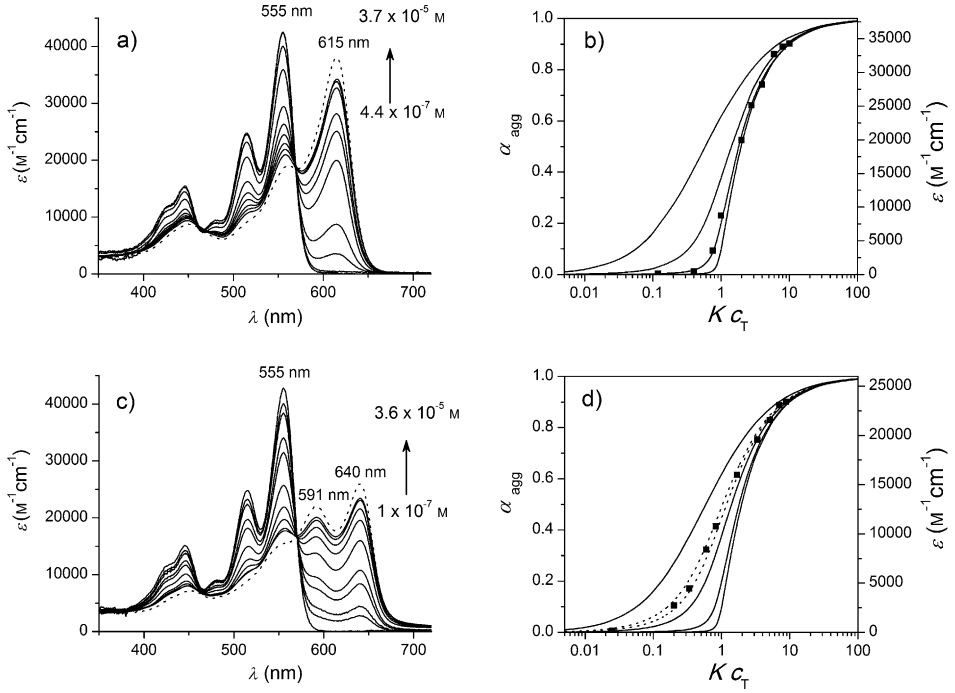

Figure 4. a,c) Concentration-dependent UV/Vis absorption spectra of a) *M*-**4** (4.4×10^{-7}–3.7×10^{-5} M, spectra for *P*-**4** are identical to those of *M*-**4**) and c) *rac*-**4** (1×10^{-7}–3.6×10^{-5} M) at 20 °C; the dotted lines show the calculated absorption spectra of the aggregates of *M*-**4** and *rac*-**4**, respectively. b, d) The fraction of aggregated molecules α_{agg} plotted as a function of Kc_T with different σ values according to cooperative nucleation-elongation model ($\sigma = 1$, 0.1, 0.01, 0.001 (solid lines from left to right), $\sigma = 0.3$ (left dotted line in (d), $\sigma = 0.2$ (right dotted line in (d)), and plots of experimental absorption data (filled squares) of *M*-**4** in MCH at 615 nm (b) and *rac*-**4** in MCH at 640 nm (d) after manual fit to the line shape. (For the method to obtain the curves with different σ values, see Ref. [19b])

CD spectra: The CD spectra of the isolated enantiomers of PBI **4** in chloroform show a clear mirror image relation as depicted in Figure 5 (black solid lines). In the region of 480–610 nm of the CD spectra, a broad monosignated peak with a maximum at 570 nm can be seen which nicely correlates with the absorption maximum

Table 1. Results of manual fitting in Figure 4b and d for aggregates of *M*-**4** and *rac*-**4** in MCH at 20 °C.

	σ	K_2	K
M-**4**	0.01	2.7×10^3	2.7×10^5
rac-**4**	0.25	6.3×10^4	2.5×10^5

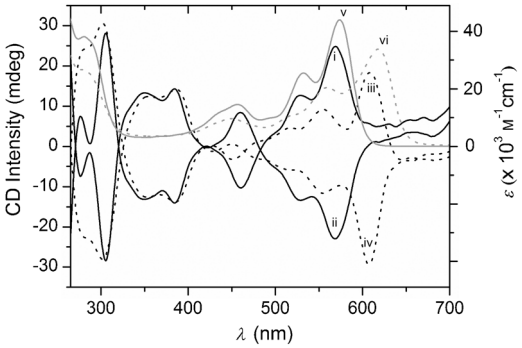

Figure 5. CD spectra of chloroform solutions of i) the first eluted fraction (*P*-**4**), ii) the second eluted fraction (*M*-**4**), and aggregates in MCH of iii) *P*-**4** and iv) *M*-**4** at 20 °C. The absorption spectra (grey lines) of v) monomeric *P*-**4** in chloroform solution and vi) its aggregate in MCH are given for reference.

Fluorescence properties: As shown in Figure 6, the molecularly dissolved *rac*-**4** in toluene exhibits a typical fluorescence spectrum of aryloxy-substituted PBIs with a maximum

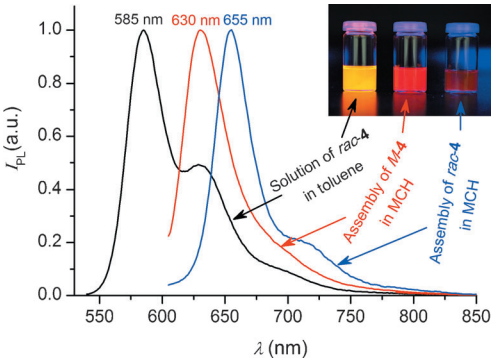

Figure 6. Normalized photoluminescence spectra of molecularly dissolved *rac*-**4** in toluene (black line, λ_{ex}: 530 nm), aggregates of *M*-**4** in MCH (red line, λ_{ex}: 600 nm) and aggregates of *rac*-**4** in MCH (blue line, λ_{ex}: 600 nm) at room temperature. Note that for the cases of *M*-**4** and *rac*-**4** in MCH only the aggregates could be excited by 600 nm light. Inset shows the photograph of *rac*-**4** in toluene (left), *M*-**4** in MCH (middle) and *rac*-**4** in MCH (right) under UV irradiation ($c=3\times10^{-5}$ M for all samples).

at 573 nm (Figure 5, gray solid line). In the CD spectral region of 480–610 nm of the enantiomers, the S_0–S_1 transition is located whose transition dipole moment is polarized along the long axis (N–N axis) of the perylene bisimide.[26] On the basis of previously reported stereochemical assignment of atropisomerically pure macrocyclic PBI systems,[14] the positive signal for the longest wavelength transition ($\lambda_{max}=570$ nm) in the CD spectrum of the first eluted fraction of PBI **4** can be attributed to a right-handed helical configuration of the twisted perylene core, and thus this enantiomer can be assigned to *P*-**4**. Accordingly, the second eluted fraction with a negative Cotton effect for the longest wavelength transition can be assigned to *M*-**4**.

When the solvent is changed to MCH, J-aggregate formation is also revealed by the CD spectra of the enantiopure PBI **4** samples (Figure 5, black dotted lines). The CD spectra of the aggregates of *P*-**4** and *M*-**4** in MCH show positive and negative Cotton effects (Figure 5, black dotted lines) in the J-absorption band range (580~640 nm, gray dotted line), indicating the helical core-twisted molecular structure present in the aggregate. The signals in the S_0–S_1 transition range (480~610 nm, black dotted lines) are monosignated, which implies that the transition dipole moments of the S_0–S_1 transition of the molecules are parallel in aggregates. Thus, there is no chiral excitonic coupling of these transition dipole moments.[27] On the other hand, bisignated signals are observed in the range of S_0–S_2 transition (420~480 nm, black dotted lines) that is perpendicular to the S_0–S_1 transition, which means that the transition dipole moment of the S_0–S_2 transition exhibit chiral excitonic coupling owing to their helical displacement. It is to note that the aggregates of *rac*-**4** are CD silent.

around 580 nm. In contrast, the fluorescence spectra of the aggregates of *M*-**4** and *rac*-**4** show pronounced bathochromic shifts of 45 nm and 70 nm, respectively, compared with that of monomers, which corresponds well to the red-shift of the absorption spectra of these aggregates. Accordingly, the Stokes shift between fluorescence and absorption maxima is reduced from 30 nm for the monomeric dye to only 15 nm each for both *M*-**4** and *rac*-**4** J-aggregates. The bathochromic shift of the photoluminescence spectrum from the aggregate of *M*-**4** to the aggregate of *rac*-**4** provides further indication for a different molecular packing arrangement in aggregates of enantiopure and racemic PBI **4**. The photoluminescence quantum yield of the aggregate of *M*-**4** was determined as high as 47±3% (the same result was obtained for the aggregate of *P*-**4**), which is much higher than that of the aggregate of *rac*-**4** (12±3%).

Morphological properties of the homochiral and heterochiral aggregates: As discussed above, PBI **4** possesses an asymmetric and twisted perylene core structure with one shielded π-surface and one π-surface being free, which result in a predominant intermolecular π–π interaction between the free π-surfaces of the adjacent molecules in aggregate and slipped molecular arrangement along the N–N molecular axis. Here we need to keep in mind that for the enantiopure PBI **4** (*M*-**4** or *P*-**4**), only homochiral aggregates could be formed; however, for the racemate of PBI **4** (*rac*-**4**) there are possibilities to form heterochiral aggregates between different enantiomeric molecules or homochiral aggregates of the same enantiomeric molecules.

To investigate the morphological properties of the aggregates from the enantiopure and racemic PBI **4**, the aggre-

gates of *M*-**4**, *P*-**4** and *rac*-**4** formed in MCH were transferred to substrates by spin-coating method, followed by AFM imaging. As shown in Figure 7a and c, very long nanowires (>5 μm) are formed based on enantiopure *M*-**4** and *P*-**4**. The nanowires formed from both enantiomers possess uniform height of 3.0±0.3 nm and width of 14±2 nm, and nicely resolved segmented structure (segment periodicity: 10±0.5 nm) was observed by AFM in phase image as depicted in Figure 7b. Moreover, cross points of two nanowires are observed as shown in Figure 7c. The height of the cross points is obviously higher than the nanowires, which excludes the branched structure of the nanowires. In contrast, AFM images of the aggregates of *rac*-**4** only shows particle-like domains with irregular size ranging from tens to hundreds of nanometers (Figure 7d). The totally different morphologies of the aggregates obtained from enantiopure *M*-**4** (or *P*-**4**) and *rac*-**4** clearly indicate the predominant formation of heterochiral aggregate for *rac*-**4**, which is in good agreement with the results of our UV/Vis studies. A similar behavior has recently been observed by Takeuchi and coworkers[16e] for helicene derivatives whose self-assembly is driven, as in our present case, by a combination of hydrogen bonding and π–π-stacking interactions. Here, like in our case, extended and defined 1D helical nanofibers were only formed for enantiopure samples, whereas ill-defined smaller aggregates were observed for the racemates.

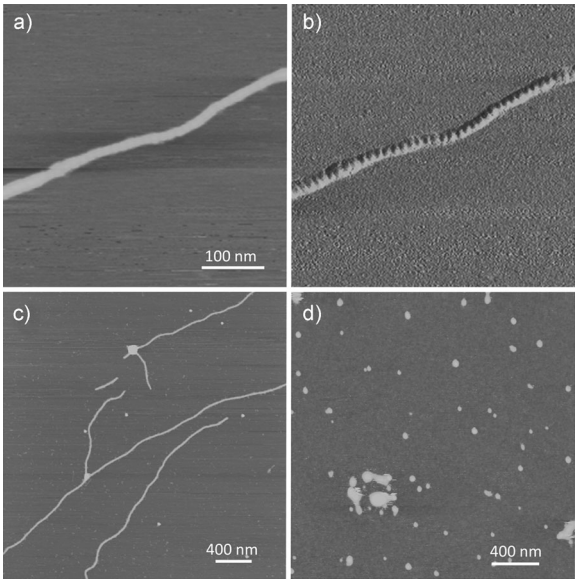

Figure 7. a,c,d) AFM height images, and b) phase image of samples spin-coated from MCH solutions (ca. 5×10^{-5} M) for the aggregates of *M*-**4** (a, b), *P*-**4** (c), and *rac*-**4** (d) on mica. Z scale for height images is 10 nm.

Aggregate model of enantiopure PBI 4: As concluded from the crystallographic and ^{1}H NMR data (Figure 2 and Figure 3), PBI **4** possesses an asymmetric molecular structure in which the biphenoxy bridge locates at one side of the perylene core and thus shields one of its π-surfaces. Obviously, the π–π interaction between two free π-surfaces of adjacent molecules should be favored, while the further growth of the aggregate along π–π stacking direction should be prohibited for the shielded π-surface. The twisted molecular structure makes it impossible to form sandwich-type face-to-face π-stacks, but a slipped arrangement along the molecular long axis (N–N direction, that is, dipole transition direction) can be easily adopted. A slipped molecular stacking is typical for J-type aggregate, which is confirmed for PBI **4** by the concentration-dependent absorption spectra (Figure 4a,c). The intermolecular hydrogen bonding (N–H···O) will direct the elongation of the aggregate, and the left or right-handed configuration of the enantiopure compound ensures the formation of helical structure. Thus, a most possible aggregate model for enantiopure PBI **4** is proposed in Figure 8, where two molecular strings with same helicity entangle each other. The driving forces are the π–π interactions between the molecules in different molecular strings and directional hydrogen bonding within each string. As estimated from the single crystal structure of bi-

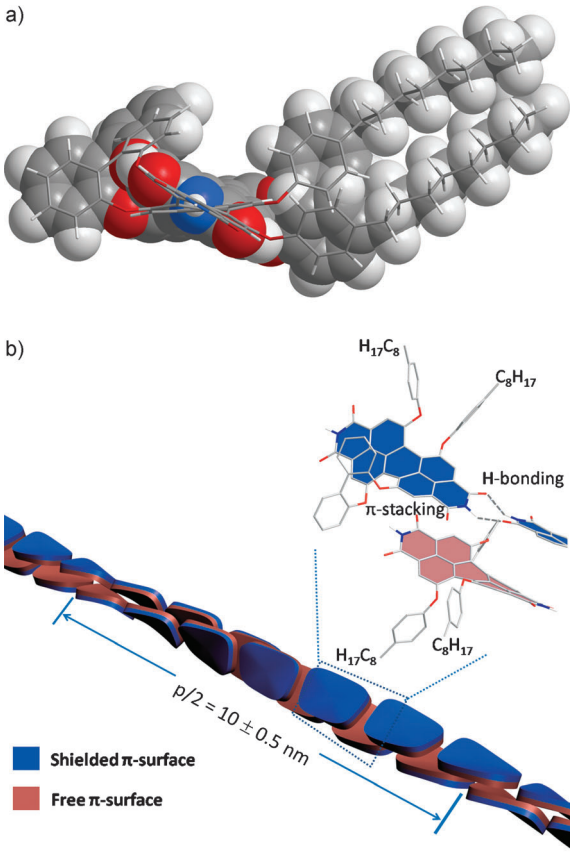

Figure 8. a) Molecular conformation of PBI **4** (*M*-enantiomer is shown here) optimized by using HyperChem 8.0 (molecular mechanics optimization, MM+ force field); for details, see the Supporting Information. b) Schematic representation for the aggregate of the enantiopure PBI (*M*-**4**). Directional hydrogen bonding dominate the elongation of the nanowires and the π-stacking interactions between two free π-surfaces are favored, whilst further growth along the π-stacking direction is prohibited. Two different colors indicate the different π-surfaces of the perylene core.

phenoxy-bridged PBI **2′**, the dihedral angle of two naphthalene planes in PBI **4** is between 25° and 33°. Thus, the helical pitch should be about 12 times (360°/30°) of one molecular length in our model, that is, 18 nm (the molecular length is ca. 1.5 nm according to the single crystal structure of PBI **2′**). This value is in proper agreement with our experimental result determined by AFM, that is, a segment periodicity of 10 ± 0.5 nm for the nanowires.

Aggregate of racemate rac-4: From the very distinct absorption spectra of the aggregates of *M*-**4** and *rac*-**4** (Figure 4a and c), one can infer that heterochiral assemblies of *rac*-**4** prevailed over homochiral assemblies of the racemate (note that *M*-**4** alone can form only homochiral assemblies). From the analysis of the concentration-dependent UV/Vis spectra of *M*-**4** and *rac*-**4** (Figure 4b, d and Table 1), it could be concluded that the intermolecular interactions in the heterodimer nucleus are much stronger than those in the homodimer nucleus. Notably, this behavior is opposite to that observed for the dimerization of simple core-twisted homo- and heterochiral PBIs where homochiral dimer assemblies are preferred.[16a] The different self-sorting behavior can be attributed to differences in the molecular structures. PBI **4** exhibits a rigid and sterically encumbering 2,2′-biphenoxy bridge that is quite distinct from the substituents applied in the previously investigated chiral, core-twisted PBIs. In addition, the slipped arrangement required for the formation of the hydrogen-bonded chain imposes further constraint on the π–π contact surface. In particular, it prohibits π–π stacking with rotational offsets which is the energetically favored arrangement for simple PBI dimer and columnar stacks.[16a,28] As a consequence of this slipping, the π–π overlap in the homo-π-dimer becomes smaller than that in the hetero-π-dimer and different intermolecular arrangements originate for homochiral and heterochiral J-aggregates that are manifested in the different UV/Vis spectra.

To get more information on the aggregate structure of *rac*-**4**, the ROESY and COSY NMR experiments of this racemic PBI were performed at a high concentration of 45 mM in $CDCl_3$ at 298 K and the results of the ROESY NMR are displayed in Figure 9a. Clear cross-peaks could be found between H^2 and H^{11}, and between H^5 and H^8 in the ROESY spectrum (Figure 9a), while they are absent in COSY spectrum (Figure S1 in the Supporting Information). The results of COSY NMR clearly rule out the possibility that these cross-peaks are originated from the indirect long-range coupling between H^2 and H^{11} (or between H^5 and H^8) protons through the aromatic naphthalene unit. Therefore, these cross-peaks must originate from the intermolecular interactions in the aggregate. On the basis of the results of UV/Vis absorption and NMR studies, we propose a model for the heteroaggregate shown in Figure 9b. It is to note that the rigid biphenoxy bridges of PBI **4** molecules locate at one side in the aggregate, while the aryloxy substituents are on the opposite side. The unsymmetric aggregate structure of the hetero-π-dimer (π-stacked pairs of molecules in Figure 9b) may influence the elongation of the aggregate to

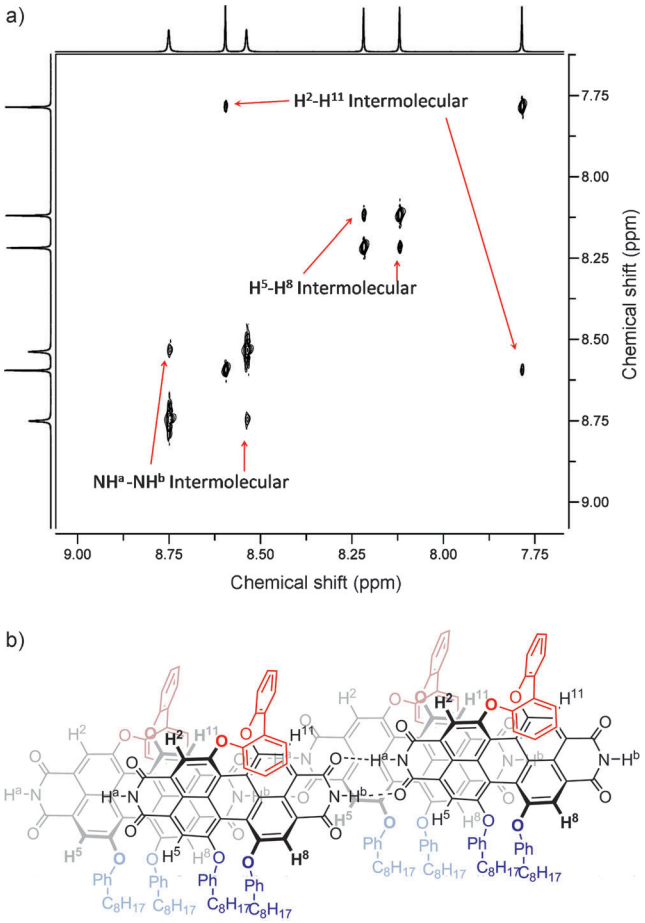

Figure 9. a) 600 MHz ROESY NMR spectrum of *rac*-**4** in $CDCl_3$ at 298 K ($c = 45$ mM). b) A structural model proposed for the heterochiral aggregate derived from the ROESY NMR. Notes to the aggregation model: the π–π overlap in a hetero-π-dimer (left or right pair) is larger than half of the π-surface of perylene bisimide core; the interactions between two adjacent hetero-π-dimers are mainly due to the multiple hydrogen bonding.

form flexural-shaped aggregates. The interactions between the two adjacent hetero-π-dimers are mainly attributed to the multiple hydrogen bonding (N–H···O), which also induce different elongation process for *rac*-**4** in comparison with that of enantiopure *M*-**4** (or *P*-**4**). The existence of intermolecular hydrogen bonding in the aggregate can be concluded from the cross-peaks between NH^a and NH^b as shown in Figure 9a. The unsymmetric location of the bay-area substituents and also the multiple intermolecular interactions result in irregular-sized, particle-like aggregates as we observed by AFM for *rac*-**4** (Figure 7d). The proposed aggregate model for the racemate can be used to explain its absorption spectrum. As mentioned before, we have observed two distinct J-bands (Figure 4c) for the aggregate of *rac*-**4**, which clearly indicate two excitonic states with allowed optical transitions both shifted towards lower energies compared to the monomer transition. The two excitonic states may relate to the exciton coupling between two adjacent molecules with the same or opposite chirality (so called

Davydov coupling originated from more than one molecule in one unit cell in crystal).[29]

Fluorescence enhancement of homochiral aggregates: The fluorescence efficiency of the helical aggregate of enantiopure *M*-**4** (nanowire) is 47±3%, which is four times higher than that of the aggregate of *rac*-**4** (particles) (12±3%). Considering the morphologies of these two types of aggregates, the fluorescence enhancement of homochiral aggregates may be attributed to the highly ordered molecular stacking in the one-dimensional nanowires. In the one-dimensional ordered structure, there should be few energy trapping sites and the exciton can only diffuse along the nanowire, which ensure the high luminescence efficiency. However, in the particle-like aggregate of *rac*-**4**, the co-aggregation of building blocks with opposite chirality may result in more disordered structures, and hence larger amount of energy trapping sites may be created. Moreover, the three-dimensional aggregation structure may facilitate the exciton migration to the energy trapping sites, and thus the exciton is quenched more easily.

Conclusion

A novel asymmetric perylene bisimide containing NH groups in the imide positions was synthesized by introducing a biphenoxy bridge at one of the bay areas. The introduction of the biphenoxy bridge renders rigidity to the perylene core, which enables easy resolution of the two atropo-enantiomers (*M* and *P*) at room temperature. The racemization process of the enantiomers is prohibited in aggregate due to intermolecular π–π stacking and hydrogen-bonding interactions. The biphenoxy bridge shields one of the π-surfaces of the perylene core, and thus prevents aggregation into columnar stacks. For the enantiopure perylene bisimide (*M*-**4** or *P*-**4**), the mutual effects of hydrogen bonding and π–π interaction restricted to one π-face resulting in the formation of well-defined extended one-dimensional nanowires with J-type excitonic coupling. On the other hand, for the racemate (*rac*-**4**) self-discrimination of the enantiomers prevails over self-recognition, that is, an enantiomer preferentially recognizes its mirror image, which results in the formation of structurally quite distinct particle-like aggregates. The highly ordered molecular arrangement in the one-dimensional homochiral nanowires ensures its enhanced luminescence efficiency in contrast to the disordered aggregate structure of the racemate. To the best of our knowledge, we have presented here the first examples of homochiral J-aggregates created by self-assembly of core-chiral π-scaffolds. Our novel results clearly show the importance of the enantiopure building blocks for the construction of highly ordered chiral nanostructures with unique optical properties as required for various kinds of optoelectronic applications.[30]

Experimental Section

All chemicals and reagents were used as received, unless otherwise stated. Column chromatography was performed using silica gel (Si60, mesh size 40–63 μm). ^{1}H NMR spectra were recorded with Bruker Avance 400 MHz and Bruker DMX 600 MHz instruments. High resolution mass spectra (HRMS) were recorded on a MicroTOF Focus from Bruker Daltonics. Analytical HPLC was carried out on a JASCO system (PU 2080 PLUS) with a diode array detector (MD 2015), equipped with a ternary gradient unit (DG-2080–533) and inline-degasser (LG 2080–02). Semi-preparative HPLC was performed on a JASCO system (PU 2080 PLUS) with an UV/Vis detector (UV 2077 PLUS). AFM measurements were performed under ambient conditions using a Veeco Multimode Nanoscope IV system operating in tapping mode in air. Silica cantilevers (OMCL-AC160TS) with a resonance frequency of about 300 kHz were used.

X-ray analysis: The synthesis and characterization data of PBI **2′** were reported previously.[17] The crystal data of PBI **2′** were collected with a Bruker X8 APEX diffractometer using CCD area detector and multilayer mirror monochromated $Mo_{K\alpha}$ radiation. The structure was solved using direct methods and expanded by applying Fourier techniques.[31] All nonhydrogen atoms were refined anisotropically. Hydrogen atoms were assigned to idealized positions and were included in structure factor calculations. CCDC-848074 (PBI **2′**) contains the supplementary crystallographic data for this paper. These data can be obtained free of charge from The Cambridge Crystallographic Data Centre via www.ccdc.cam.ac.uk/data_request/cif.

UV/Vis absorption, fluorescence, and circular dichroism (CD) spectroscopy: For all spectroscopic measurements, spectroscopic grade solvents (Uvasol®) were used. UV/Vis spectra were recorded with a Perkin–Elmer Lambda 950 spectrometer equipped with a PTP-1 Peltier element. CD spectra were measured with a JASCO J-810 spectrometer equipped with a CDF-242 Peltier element. Fluorescence spectra were recorded with a PTI QM-4/2003 instrument. All fluorescence measurements were performed at room temperature and the spectra were corrected against photomultiplier and lamp intensity. The fluorescence quantum yields were determined as the average value for three different excitation wavelengths using *N*,*N*′-bis(2,6-diisopropylphenyl)-1,6,7,12-tetraphenoxy-perylene-3,4:9,10- tetracarboxylic acid bisimide ($\Phi_{Fl}=0.96$ in $CHCl_3$) by applying high dilution conditions ($A<0.05$).[32]

Synthesis of PBI 2: A portion of 1.47 g (2.0 mmol) of *N*,*N*′-bis(α-methylbenzyl)-1,6,7,12-tetrachloroperylene-3,4:9,10-tetracarboxylic acid bisimide (PBI **1**), 410 mg (2.2 mmol) of 2,2′-biphenol and 304 mg (2.2 mmol) K_2CO_3 were suspended in 80 mL of *N*-methyl-2-pyrrolidone (NMP) and stirred under argon at 120 °C for 40 h. After being cooled to room temperature, the reaction mixture was dropped into 300 mL of 1 N HCl under stirring. The precipitate was separated by filtration and washed successively with water (3×50 mL) and methanol (3×50 mL). The crude product was purified by column chromatography on silica gel using CH_2Cl_2/*n*-hexane (70:30) as an eluent. After removal of the solvent with rotary evaporator, 730 mg (44% yield) of PBI **2** were obtained. ^{1}H NMR (400 MHz, $CDCl_3$): $\delta=8.66$–8.60 (m, 2H), 8.50–8.46 (m, 1H), 7.83 (m, 1H), 7.60–7.20 (m, 15H), 6.88 (m, 1H), 6.77 (m, 1H), 6.58 (q, $J=7.3$ Hz, 1H), 6.41 (q, $J=7.1$ Hz, 1H), 6.20 (m, 1H), 2.03 (dd, 3H), 1.92 ppm (d, 3H); ^{13}C NMR (100 MHz, CD_2Cl_2): $\delta=162.1$, 162.0, 161.95, 161.88, 161.78, 161.74, 161.7, 161.62, 155.55, 153.71, 151.83, 151.82, 150.15, 139.93, 139.78, 139.73, 134.03, 133.97, 131.89, 131.26, 131.21, 130.58, 130.53, 130.41, 130.36, 130.08, 129.83, 129.82, 129.23, 129.19, 129.0, 128.86, 128.39, 127.51, 127.5, 127.49, 127.36, 127.33, 127.29, 127.24, 126.27, 126.25, 126.17, 126.11, 125.46, 124.33, 124.28, 123.05, 122.71, 122.68, 122.55, 122.1, 120.91, 120.26, 119.72, 119.68, 119.6, 119.57, 118.31, 118.25, 115.95, 49.82, 49.76, 49.72, 15.36, 15.27, 15.25, 15.17 ppm; UV/Vis ($CHCl_3$): λ_{max} (ε_{max})= 549 nm (40 000 $M^{-1}cm^{-1}$); fluorescence ($CHCl_3$, $\lambda_{ex}=530$ nm): $\lambda_{max}=$ 571 nm, $\Phi_{Fl}=0.86\pm0.01$; HRMS (ESI, $CHCl_3$/acetonitrile 1:1, pos. mode): *m*/*z* calcd for $C_{52}H_{31}Cl_2N_2O_6$, 849.1559 $[M+H]^+$; found: 849.1551.

Synthesis of PBI 3: A portion of 255 mg (0.30 mmol) of PBI **2**, 186 mg (0.90 mmol) of 4-*tert*-butylphenol and 62.2 mg (0.45 mmol) of K_2CO_3 were suspended in 10 mL of NMP and stirred under argon at 120 °C for

24 h. After being cooled to room temperature, the reaction mixture was dropped into 100 mL NaCl(aq), then extracted with $CHCl_3$ (2×50 mL). The organic layer was washed with water (3×100 mL), and dried over Na_2SO_4. The crude product was purified by column chromatography on silica gel using CH_2Cl_2/*n*-hexane (60:40) as an eluent. After removing the solvent with rotary evaporator, 150 mg (42% yield) of PBI **3** was obtained. ^{1}H NMR (400 MHz, CD_2Cl_2): δ = 8.44 (m, 1H), 8.01 (m, 1H), 7.88 (m, 1H), 7.64 (m, 1H), 7.51 (m, 1H), 7.44 (m, 1H), 7.40–7.32 (m, 3H), 7.31–7.02 (m, 10H), 6.95 (m, 4H), 6.80 (m, 1H), 6.75–6.65 (m, 5H), 6.40 (q, J = 6.8 Hz, 1H), 6.21 (m, 2H), 2.45 (m, 4H), 1.86 (d, 3H), 1.73 (d, 3H), 1.47 (brs, 4H), 1.24 (m, 20H), 0.81 ppm (m, 4H); ^{13}C NMR (100 MHz, CD_2Cl_2): δ = 163.71, 163.59, 163.56, 163.48, 163.41, 163.37, 163.32, 163.22, 156.64, 156.54, 156.27, 154.51, 154.49, 153.65, 153.62, 153.58, 153.49, 153.47, 153.43, 153.41, 153.27, 151.62, 141.4, 141.35, 141.24, 141.16, 139.9, 139.89, 133.59, 133.57, 131.66, 131.62, 131.57, 131.51, 131.07, 130.12, 130.06, 128.96, 128.57, 128.54, 128.45, 128.41, 128.39, 128.32, 127.38, 127.25, 127.18, 126.33, 125.78, 125.22, 125.18, 123.89, 123.84, 123.41, 123.36, 123.32, 123.29, 122.16, 121.63, 121.59, 121.27, 120.85, 120.72, 120.7, 120.63, 120.61, 120.53, 120.48, 120.28, 120.26, 120.19, 120.08, 119.91, 119.81, 119.45, 119.34, 119.31, 116.97, 50.63, 50.61, 50.57, 50.52, 35.61, 32.35, 32.03, 29.89, 29.76, 29.72, 23.11, 16.46, 16.39, 16.33, 16.28, 14.29 ppm; UV/Vis ($CHCl_3$): λ_{max} (ε_{max}) = 576 nm (51 300 M^{-1}cm^{-1}); fluorescence ($CHCl_3$, λ_{ex} = 530 nm): λ_{max} = 597 nm, Φ_{Fl} = 0.94 ± 0.01; HRMS (ESI, $CHCl_3$/acetonitrile 1:1, pos. mode): m/z calcd for $C_{80}H_{73}N_2O_8$, 1189.5367 $[M+H]^+$; found: 1189.5378.

Synthesis of the target PBI 4: A mixture of 95 mg (0.08 mmol) of PBI **3** and 1.0 g (18.0 mmol) of solid KOH in 15 mL of *t*BuOH was heated to 80 °C for 3 h. After being cooled to room temperature, the reaction mixture was dropped into 50 mL glacial acetic acid under stirring. Then 200 mL water was added to dilute the mixture. The crude product was extracted with 50 mL $CHCl_3$, and then the organic layer was separated and washed successively with water (100 mL), $NaHCO_3$ (aq) (100 mL), and again water (2×100 mL). The chloroform solution was dried over Na_2SO_4 and the solvent was removed with rotary evaporator. The residual solid was dissolved in 20 mL propionic acid together with 2.0 g of ammonium acetate. The mixture was stirred at 140 °C for 60 h. After cooling to room temperature, the mixture was added dropwise into 200 mL water under stirring. The crude product was extracted with chloroform (2× 50 mL) and the organic solution was dried over $MgSO_4$. After removing the solvent, the residue was purified by column chromatography on silica gel using chloroform as an eluent. After rotatory evaporation of the solvent, the product was dried under vacuum (70 °C, 10^{-3} mbar, SiO_2) to obtain 64 mg (82% yield) of pure PBI **4**. ^{1}H NMR (c = 45 mM, 600 MHz, $CDCl_3$): δ = 8.75 (s, 1H), 8.60 (s, 1H), 8.54 (s, 1H), 8.22 (s, 1H), 8.12 (s, 1H), 7.79 (s, 1H), 7.60 (d, J = 7.7 Hz, 1H), 7.54 (t, J = 7.7 Hz, 1H), 7.47 (t, J = 7.6 Hz, 1H), 7.37 (d, J = 7.8 Hz, 1H), 7.34 (d, J = 7.7 Hz, 1H), 7.03 (m, 4H), 6.90 (t, J = 7.5 Hz, 1H), 6.83 (d, J = 8.4 Hz, 2H), 6.79 (t, J = 7.8 Hz, 1H), 6.75 (d, J = 8.6 Hz, 2H), 6.28 (d, J = 8.2 Hz, 1H), 2.54 (m, 4H), 1.57 (m, 4H), 1.32 (m, 20H), 0.90 ppm (m, 6H); ^{13}C NMR (100 MHz, $CDCl_3$): δ = 163.14, 163.04, 162.93, 162.87, 156.37, 156.33, 156.12, 154.17, 153.07, 152.95, 152.71, 151.19, 139.66, 133.7, 131.76, 131.27, 130.88, 129.92, 129.86, 128.75, 128.12, 126.24, 125.47, 125.2, 123.1, 123.02, 122.6, 122.48, 122.01, 121.86, 121.67, 120.99, 120.75, 120.51, 120.23, 120.17, 119.92, 119.76, 119.63, 118.95, 116.62, 35.42, 32.08, 31.72, 31.7, 29.65, 29.51, 29.46, 22.84, 14.26 ppm; UV/Vis ($CHCl_3$): λ_{max} (ε_{max}) = 574 (44 000), 532 (25 500), 456 nm (14 600 M^{-1}cm^{-1}); fluorescence: λ_{max} ($CHCl_3$, 25 °C, λ_{ex} = 530 nm) = 596 nm, Φ_{Fl} ($CHCl_3$, 25 °C) = 0.94 ± 0.01, λ_{max} (MCH, 60 °C) = 568 nm, Φ_{Fl} (MCH, 60 °C, λ_{ex} = 530 nm) = 1.00 ± 0.01; HRMS (ESI, $CHCl_3$/acetonitrile 1:1, pos. mode): m/z calcd for $C_{64}H_{57}N_2O_8$, 981.4115 $[M+H]^+$; found: 981.4107.

Resolution of atropo-enantiomers (*P*-4 and *M*-4) by HPLC: Separation of the enantiomers was achieved on a semi-preparative column (Trentec Reprosil 100 chiral-NR, Ø = 2.5 cm) using chloroform as an eluent (flow: 8.0 mL min^{-1}). The retention times for the first and second eluted atropo-enantiomers are 17 min and 25 min, respectively.

Preparation of aggregates in methylcyclohexane (MCH): The aggregates of both enantiopure and racemic PBI **4** were prepared by injecting the concentrated chloroform solutions (3.8×10^{-3} M) into MCH, followed by ultrasonic treatment for half a minute to give a homogenous mixture. The aggregates in MCH with different concentrations were kept at room temperature in 5 mL vials overnight to reach the equilibrium between the monomers and aggregates. Then the samples were shaken for about 10 seconds and then transferred into quartz cells for UV/Vis absorption and fluorescence measurements. For AFM measurements, the aggregates prepared in MCH with a concentration of about 5×10^{-5} M was shaken for about 10 seconds and then drop-cast onto muscovite mica or Si-wafer (SiO_x) surfaces. After approximately 30 seconds, the solvent was removed by spinning for one minute (7000 r min^{-1}).

Acknowledgements

We thank the Alexander von Humboldt Foundation for a postdoctoral fellowship for Z.X.

[1] For reviews, see: a) *J-Aggregates*, (Ed: T. Kobayashi), World Scientific, Singapore, **1996**; b) D. Möbius, *Adv. Mater.* **1995**, *7*, 437–444; c) K. C. Hannah, B. A. Armitage, *Acc. Chem. Res.* **2004**, *37*, 845–853; d) S. Kirstein, S. Dähne, *Int. J. Photoenergy* **2006**, *5*, 3; e) F. C. Spano, *Acc. Chem. Res.* **2010**, *43*, 429–439; f) F. Würthner, T. E. Kaiser, C. R. Saha-Möller, *Angew. Chem.* **2011**, *123*, 3436–3473; *Angew. Chem. Int. Ed.* **2011**, *50*, 3376–3410.

[2] a) K. E. Achyuthan, T. S. Bergstedt, L. Chen, R. M. Jones, S. Kumaraswamy, S. A. Kushon, K. D. Ley, L. Lu, D. McBranch, H. Mukundan, F. Rininsland, X. Shi, W. Xia, D. G. Whitten, *J. Mater. Chem.* **2005**, *15*, 2648–2656; b) D. G. Whitten, K. E. Achyuthan, G. P. Lopez, O. K. Kim, *Pure Appl. Chem.* **2006**, *78*, 2313–2323.

[3] D. M. Eisele, H. V. Berlepsch, C. Böttcher, K. J. Stevenson, D. A. Vanden Bout, S. Kirstein, J. P. Rabe, *J. Am. Chem. Soc.* **2010**, *132*, 2104–2105.

[4] a) E. Lang, A. Sorokin, M. Drechsler, Y. V. Malyukin, J. Köhler, *Nano Lett.* **2005**, *5*, 2635–2640; b) H. Lin, R. Camacho, Y. Tian, T. E. Kaiser, F. Würthner, I. G. Scheblykin, *Nano Lett.* **2010**, *10*, 620–626.

[5] a) C. Spitz, S. Dähne, A. Ouart, H.-W. Abraham, *J. Phys. Chem. B* **2000**, *104*, 8664–8669; b) A. Chowdhury, S. Wachsmann-Hogiu, P. R. Bangal, I. Raheem, L. A. Peteanu, *J. Phys. Chem. B* **2001**, *105*, 12196–12201; c) O.-K. Kim, J. Je, G. Jernigan, L. Buckley, D. Whitten, *J. Am. Chem. Soc.* **2006**, *128*, 510–516; d) H. Görner, T. D. Slavnova, A. K. Chibisov, *J. Phys. Chem. B* **2010**, *114*, 9330–9337; e) T. D. Slavnova, H. Görner, A. K. Chibisov, *J. Phys. Chem. B* **2011**, *115*, 3379–3384.

[6] a) O. Ohno, Y. Kaizu, H. Kobayashi, *J. Chem. Phys.* **1993**, *99*, 4128–4139; b) J. M. Ribó, J. Crusats, F. Sagués, J. Claret, R. Rubires, *Science* **2001**, *292*, 2063–2066; c) A. S. R. Koti, N. Periasamy, *Chem. Mater.* **2003**, *15*, 369–371; d) R. Lauceri, G. F. Fasciglione, A. D'Urso, S. Marini, R. Purrello, M. Coletta, *J. Am. Chem. Soc.* **2008**, *130*, 10476–10477; e) A. Mammana, G. Pescitelli, T. Asakawa, S. Jockusch, A. G. Petrovic, R. R. Monaco, R. Purrello, N. J. Turro, K. Nakanishi, G. A. Ellestad, M. Balaz, N. Berova, *Chem. Eur. J.* **2009**, *15*, 11853–11866; f) A. D'Urso, A. Mammana, M. Balaz, A. E. Holmes, N. Berova, R. Lauceri, R. Purrello, *J. Am. Chem. Soc.* **2009**, *131*, 2046–2047; g) M. A. Castriciano, A. Roemo, G. De Luca, V. Villari, L. M. Scolaro, N. Micali, *J. Am. Chem. Soc.* **2011**, *133*, 765–767.

[7] a) T. S. Balaban, H. Tamiaki, A. R. Holzwarth, *Top. Curr. Chem.* **2005**, *258*, 1–38; b) V. Huber, M. Katterle, M. Lysetska, F. Würthner, *Angew. Chem.* **2005**, *117*, 3208–3212; *Angew. Chem. Int. Ed.* **2005**, *44*, 3147–3151; c) V. Huber, S. Sengupta, F. Würthner, *Chem. Eur. J.* **2008**, *14*, 7791–7807.

[8] a) J.-S. Zhao, Y.-B. Ruan, R. Zhou, Y.-B. Jiang, *Chem. Sci.* **2011**, *2*, 937–944; b) F. Würthner, C. Bauer, V. Stepanenko, S. Yagai, *Adv. Mater.* **2008**, *20*, 1695–1698.

[9] A. R. A. Palmans, E. W. Meijer, *Angew. Chem.* **2007**, *119*, 9106–9126; *Angew. Chem. Int. Ed.* **2007**, *46*, 8948–8968.
[10] For reviews on self-assembly of π-conjugated systems, see: a) F. J. M. Hoeben, P. Jonkheijm, E. W. Meijer, A. P. H. J. Schenning, *Chem. Rev.* **2005**, *105*, 1491–1546; b) D. B. Amabilino, J. Veciana, *Top. Curr. Chem.* **2006**, *265*, 253–302; c) M. R. Wasielewski, *J. Org. Chem.* **2006**, *71*, 5051–5066; d) A. Ajayaghosh, V. K. Praveen, *Acc. Chem. Res.* **2007**, *40*, 644–656; e) L. Zang, Y. Che, J. S. Moore, *Acc. Chem. Res.* **2008**, *41*, 1596–1608; f) D. González-Rodríguez, A. P. H. J. Schenning, *Chem. Mater.* **2011**, *23*, 310–325; g) F. S. Kim, G. Ren, S. A. Jenekhe, *Chem. Mater.* **2011**, *23*, 682–732; h) B. Rybtchinski, *ACS Nano* **2011**, *5*, 6791–6818.
[11] a) J. H. Ky Hirschberg, L. Brunsveld, A. Ramzi, J. A. J. M. Vekemans, R. Sijbesma, E. W. Meijer, *Nature* **2000**, *407*, 167–170; b) J. J. L. M. Cornelissen, A. E. Rowan, R. J. M. Nolte, N. A. J. M. Sommerdijk, *Chem. Rev.* **2001**, *101*, 4039–4070; c) A. Ajayaghosh, P. Chithra, R. Varghese, *Angew. Chem.* **2007**, *119*, 234–237; *Angew. Chem. Int. Ed.* **2007**, *46*, 230–233; d) P. Chithra, R. Varghese, K. P. Divya, A. Ajayaghosh, *Chem. Asian J.* **2008**, *3*, 1365–1373; e) D. K. Smith, *Chem. Soc. Rev.* **2009**, *38*, 684–694; f) C. C. Lee, C. Grenier, E. W. Meijer, A. P. H. J. Schenning, *Chem. Soc. Rev.* **2009**, *38*, 671–683; g) Y. Hizume, K. Tashiro, R. Charvet, Y. Yamamoto, A. Saeki, S. Seki, T. Aida, *J. Am. Chem. Soc.* **2010**, *132*, 6628–6629; h) I. Danila, F. Riobé, F. Piron, J. Puigmartí-Luis, J. D. Wallis, M. Linares, H. Ågren, D. Beljonne, D. B. Amabilino, N. Avarvari, *J. Am. Chem. Soc.* **2011**, *133*, 8344–8353.
[12] a) F. Würthner, *Pure Appl. Chem.* **2006**, *78*, 2341–2349; <*lit* b> A. C. Grimsdale, K. Müllen, *Angew. Chem.* **2005**, *117*, 5732–5772; *Angew. Chem. Int. Ed.* **2005**, *44*, 5592–5629.
[13] P. Osswald, F. Würthner, *J. Am. Chem. Soc.* **2007**, *129*, 14319–14326.
[14] P. Osswald, M. Reichert, G. Bringmann, F. Würthner, *J. Org. Chem.* **2007**, *72*, 3403–3411.
[15] For a recent review on self-sorting phenomena in supramolecular systems, see: a) M. M. Safont-Sempere, G. Fernández, F. Würthner, *Chem. Rev.* **2011**, *111*, 5784–5814. For some most recent publications dedicated to self-sorting phenomena, see: b) M. Lista, J. Areephong, N. Sakai, S. Matile, *J. Am. Chem. Soc.* **2011**, *133*, 15228–15231; c) H. Maeda, K. Kinoshita, K. Naritani, Y. Bando, *Chem. Commun.* **2011**, *47*, 8241–8243; A. Das, S. Ghosh, *Chem. Commun.* **2011**, *47*, 8922–8924; d) K. Mahata, M. Schmittel, *Beilstein J. Org. Chem.* **2011**, *7*, 1555–1561; e) M. M. Smith, D. K. Smith, *Soft Matter* **2011**, *7*, 4856–4860; f) W. Jiang, D. Sattler, K. Rissanen, C. A. Schalley, *Org. Lett.* **2011**, *13*, 4502–4505; g) W. Jiang, Q. Wang, I. Linder, F. Klautzsch, C. A. Schalley, *Chem. Eur. J.* **2011**, *17*, 2344–2348.
[16] a) M. M. Safont-Sempere, P. Osswald, M. Stolte, M. Grüne, M. Renz, M. Kaupp, K. Radacki, H. Braunschweig, F. Würthner, *J. Am. Chem. Soc.* **2011**, *133*, 9580–9591. For other examples of chiral self-sorting in π-aggregates, see: b) I. W. Hwang, T. Kamada, T. K. Ahn, D. M. Ko, T. Nakamura, A. Tsuda, A. Osuka, D. Kim, *J. Am. Chem. Soc.* **2004**, *126*, 16187–16198; c) T. Kamada, N. Aratani, T. Ikeda, N. Shibata, Y. Higuchi, A. Wakamiya, S. Yamaguchi, K. S. Kim, Z. S. Yoon, D. Kim, A. Osuka, *J. Am. Chem. Soc.* **2006**, *128*, 7670–7678; d) M. Mizumura, H. Shinokubo, A. Osuka, *Angew. Chem.* **2008**, *120*, 5458–5461; *Angew. Chem. Int. Ed.* **2008**, *47*, 5378–5381; e) T. Kaseyama, S. Furumi, X. Zhang, K. Tanaka, M. Takeuchi, *Angew. Chem.* **2011**, *123*, 3768–3771; *Angew. Chem. Int. Ed.* **2011**, *50*, 3684–3687.
[17] Z. Xie, F. Würthner, *Org. Lett.* **2010**, *12*, 3204–3207.
[18] For recent works on distorted perylene bisimide dyes, see: a) Y. G. Zhen, W. Yue, Y. Li, W. Jiang, S. Di Motta, E. Di Donato, F. Negri, S. Ye, Z. H. Wang, *Chem. Commun.* **2010**, *46*, 6078–6080; b) H. L. Qian, F. Negri, C. R. Wang, Z. H. Wang, *J. Am. Chem. Soc.* **2008**, *130*, 17970–17976; c) H. L. Qian, Z. H. Wang, W. Yue, D. B. Zhu, *J. Am. Chem. Soc.* **2007**, *129*, 10664–10665.
[19] a) T. E. Kaiser, H. Wang, V. Stepanenko, F. Würthner, *Angew. Chem.* **2007**, *119*, 5637–5640; *Angew. Chem. Int. Ed.* **2007**, *46*, 5541–5544; b) T. E. Kaiser, V. Stepanenko, F. Würthner, *J. Am. Chem. Soc.* **2009**, *131*, 6719–6732.
[20] G. Sheldrick, *Acta Crystallogr.* **2008**, *A64*, 112–122.
[21] F. Würthner, A. Sautter, J. Schilling, *J. Org. Chem.* **2002**, *67*, 3037–3044.
[22] F. C. De Schryver, T. Vosch, M. Cotlet, M. Van der Auweraer, K. Müllen, J. Hofkens, *Acc. Chem. Res.* **2005**, *38*, 514–522.
[23] a) P. Jonkheijm, P. van der Schoot, A. P. H. J. Schenning, E. W. Meijer, *Science* **2006**, *313*, 80–83; b) M. M. J. Smulders, A. P. H. J. Schenning, E. W. Meijer, *J. Am. Chem. Soc.* **2008**, *130*, 606–611.
[24] R. B. Martin, *Chem. Rev.* **1996**, *96*, 3043–3064.
[25] C. A. Hunter, H. L. Anderson, *Angew. Chem.* **2009**, *121*, 7624–7636; *Angew. Chem. Int. Ed.* **2009**, *48*, 7488–7499 and references therein.
[26] a) C. Huang, S. Barlow, S. R. Marder, *J. Org. Chem.* **2011**, *76*, 2386–2407; b) H. Langhals, *Heterocycles* **1995**, *40*, 477–500.
[27] a) N. Harada, K. Nakanishi, *Acc. Chem. Res.* **1972**, *5*, 257–263; b) N. Berova, L. Di Bari, G. Pescitelli, *Chem. Soc. Rev.* **2007**, *36*, 914–931.
[28] a) Z. Chen, V. Stepanenko, V. Dehm, P. Prins, L. D. A. Siebbeles, J. Seibt, P. Marquetand, V. Engel, F. Würthner, *Chem. Eur. J.* **2007**, *13*, 436–449; b) Z. Chen, U. Baumeister, C. Tschierske, F. Würthner, *Chem. Eur. J.* **2007**, *13*, 450–465.
[29] a) A. S. Davydov, *Theory of Molecular Excitons*, McGraw-Hill, New York, **1969**; b) P. Dawson, *J. Phys. Chem. Solids* **1975**, *36*, 1401–1403.
[30] *Chirality at the Nanoscale, Nanoparticles, Surfaces, Materials and more*, (Ed.: D. B. Amabilino), Wiley-VCH, Weinheim, **2009**.
[31] Z. Chen, M. G. Debije, T. Debaerdemaeker, P. Osswald, F. Würthner, *ChemPhysChem* **2004**, *5*, 137–140.
[32] a) R. Gvishi, R. Reisfeld, Z. Burshtein, *Chem. Phys. Lett.* **1993**, *213*, 338–344; b) R. Sens, K. H. Drexhage, *J. Lumin.* **1981**, *24-25*, 709–712.

Received: January 9, 2012
Revised: March 16, 2012
Published online: April 30, 2012

